

COSMIC STAR FORMATION HISTORY AND THE FUTURE OBSERVATION OF SUPERNOVA RELIC NEUTRINOS

SHIN'ICHIRO ANDO

Department of Physics, School of Science, University of Tokyo, 7-3-1 Hongo, Bunkyo-ku, Tokyo 113-0033, Japan

Submitted 2003 November 17; accepted 2004 February 3

ABSTRACT

We investigate the flux and event rate of supernova relic neutrinos (SRNs) and discuss their implications for the cosmic star formation rate. Since SRNs are diffuse neutrino background emitted from past core-collapse supernova explosions, they contain fruitful information on the supernova rate in the past and present universe, as well as on the supernova neutrino spectrum itself. As reference models, we adopt the supernova rate model based on recent observations and the supernova neutrino spectrum numerically calculated by several groups. In the detection energy range $E_e > 10$ MeV, which will possibly be a background-free region in the near future, the SRN event rate is found to be $1\text{--}2\text{ yr}^{-1}$ at a water Cerenkov detector with a fiducial volume of 22.5 kton, depending on the adopted neutrino spectrum. We also simulate the expected signal with one set of the reference models by using the Monte Carlo method and then analyze these pseudodata with several free parameters, obtaining the distribution of the best-fit values for them. In particular, we use a parameterization such that $R_{\text{SN}}(z) = R_{\text{SN}}^0(1+z)^\alpha$, where $R_{\text{SN}}(z)$ is the comoving supernova rate density at redshift z and R_{SN}^0 and α are free parameters, assuming that the supernova neutrino spectrum and luminosity are well understood by way of a future Galactic supernova neutrino burst or the future development of numerical supernova simulations. The obtained 1σ errors for these two parameters are found to be $\delta\alpha/\langle\alpha\rangle = 30\%$ (7.8%) and $\delta R_{\text{SN}}^0/\langle R_{\text{SN}}^0\rangle = 28\%$ (7.7%) for a detector with an effective volume of 22.5 kton \times 5 yr (440 kton \times 5 yr), where one of the parameters is fixed. On the other hand, if we fix neither of the values for these two parameters, the expected errors become rather large, $\delta\alpha/\langle\alpha\rangle = 37\%$ and $\delta R_{\text{SN}}^0/\langle R_{\text{SN}}^0\rangle = 55\%$, even with an effective volume of 440 kton \times 5 yr.

Subject headings: diffuse radiation — neutrinos — galaxies: evolution — supernovae: general

1. INTRODUCTION

In recent years we have made remarkable progress in our knowledge concerning how the cosmic star formation history proceeded in the past and concerning the fraction of baryons locked up in stars and gas in the local universe. These points were inferred from observations of the light emitted by stars of various masses at various wavelengths. Madau et al. (1996) investigated the galaxy luminosity density of rest-frame ultraviolet (UV) radiation up to $z \sim 4$, and they converted it into the cosmic star formation rate (SFR). The rest-frame UV light is considered to be a direct tracer of star formation because it is mainly radiated by short-lived massive stars. After the pioneering study by Madau et al., a wealth of data have become available in the form of the cosmic SFR in a wide range of redshifts; these data were inferred from observations using far-infrared (FIR)/submillimeter dust emission (Hughes et al. 1998; Flores et al. 1999) and near-infrared (NIR) $H\alpha$ line emission (Gallego et al. 1995; Gronwall 1998; Tresse & Maddox 1998; Glazebrook et al. 1999), as well as the rest-frame UV emission from massive stars (Lilly et al. 1996; Cowie et al. 1996; Connolly et al. 1997; Sawicki, Lin, & Yee 1997; Treyer et al. 1998; Madau, Pozzetti, & Dickinson 1998b; Pascarella, Lanzetta, & Fernandez-Soto 1998; Steidel et al. 1999).

In these traditional methods, however, there are a fair number of ambiguities when the actual observables are converted into the cosmic SFR (Somerville, Primack, & Faber 2001). First, observable samples are generally flux-limited, and thus the intrinsic luminosity of the faintest objects in the sample

changes with redshift. In order to understand the true redshift dependence of the total luminosity density, this incompleteness is generally corrected by using a functional form (i.e., a Schechter function) of the luminosity function obtained from the observations themselves. Unfortunately, since the luminosity function is not well established observationally (especially for high- z regions), it is uncertain whether the Schechter-function fit is good enough or not. Second, the conversion from luminosity density to SFR generally relies on stellar population models, an assumed star formation history, and an initial mass function (IMF), which are not also well established yet. Finally, if the tracer of star formation is an optical or UV luminosity, then the effects of dust extinction are nonnegligible. Although this problem is less critical in other wave bands such as NIR $H\alpha$ or FIR/submillimeter, the bulk of current data consists of rest-frame UV observations, especially of high-redshift regions. After adopting some correction law for dust extinction, the rest-frame UV data become rather consistent with $H\alpha$ or submillimeter data points; still, in this case it is unknown whether the UV and submillimeter sources are identical, which is very important for measuring the cosmic SFR.

Thus, our knowledge concerning the cosmic SFR is quite crude, and therefore another type of observation that is independent of the above methods would be very important. In this paper we consider supernova relic neutrinos (SRNs), i.e., a diffuse background of neutrinos that were emitted from past supernova explosions. Type Ib, Ic, and II supernova explosions are considered to have traced the cosmic SFR, because they are directly connected with the death of massive stars with $M \gtrsim 8M_\odot$ and their lifetime is expected to be very short compared with the time scale of star formation. These events

are triggered by gravitational collapse, and 99% of the gravitational binding energy is released as neutrinos; this basic scenario was roughly confirmed by the well-known observation of the neutrino burst from SN 1987A by the Kamiokande II and IMB detectors (Hirata et al. 1987; Bionta et al. 1987). The advantages of using SRNs to probe the cosmic SFR are as follows: First, as mentioned above, if we can probe the supernova rate from SRN observation, it can be directly transformed to the SFR assuming the IMF, because supernovae are short-lived astrophysical events. The second advantage, which is more important, is that neutrinos are completely free of dust extinction. This point is the same with observations in the submillimeter wave band; however, neutrinos are emitted directly from stars, whereas submillimeter radiation comes from dust and is an indirect process.

The SRN flux and the event rates at a currently working large-volume water Cerenkov detector, Super-Kamiokande (SK), have been investigated by many researchers using theoretically/observationally modeled SFRs (Totani & Sato 1995; Totani, Sato, & Yoshii 1996; Malaney 1997; Hartmann & Woosley 1997; Kaplinghat, Steigman, & Walker 2000; Ando, Sato, & Totani 2003). More recently, the SK collaboration obtained a 90% CL upper limit on the SRN flux, i.e., $1.2 \text{ cm}^{-2} \text{ s}^{-1}$ in the energy range $E_\nu > 19.3 \text{ MeV}$ (Malek et al. 2003). This severe constraint is only about factor of 3–6 larger than the typical theoretical models and is very useful for obtaining several rough estimations of the cosmic SFR (Fukugita & Kawasaki 2003; Strigari et al. 2003) and probing the properties of neutrinos as elementary particles (Ando & Sato 2003a; Ando 2003).

However, we need a further ~ 40 years to reduce the current limit by a factor of 3 if we use the SK detector with current performance. This is because there is no energy window for SRN detection where the SRN signal dominates other background events coming from various sources, such as solar, reactor, and atmospheric neutrinos, as well as cosmic-ray muons (Ando et al. 2003). Therefore, current observations are seriously affected by the other backgrounds and take much time to reach the required sensitivity. In order to overcome this difficulty, a very interesting and promising method was proposed to directly tag electron antineutrinos ($\bar{\nu}_e$), and it is now in the research and development phase (Beacom & Vagins 2003). The basic idea is to dissolve 0.2% gadolinium trichloride (GdCl_3) into the pure water of SK. With this mixture, 90% of the neutrons produced by the $\bar{\nu}_e p \rightarrow e^+ n$ reaction are captured on Gd and then decay with 8 MeV gamma cascades. When we detect these gamma cascades, as well as the preceding Cerenkov radiation from positrons, it indicates that these signals come from original $\bar{\nu}_e$, not from other flavor neutrinos or muons. With this method, we can remove the background signals in the energy range 10–30 MeV, in which before removal there is a huge amount of background from solar neutrinos (ν_e) and atmospheric muon-neutrinos ($\nu_\mu, \bar{\nu}_\mu$) or cosmic-ray muon induced events. Because the expected SRN rate is estimated to be $1\text{--}2 \text{ yr}^{-1}$ in the energy range 10–30 MeV, the Gd-loaded SK detector (Gd-SK) would enable us to detect a few SRN events each year.

Therefore, it is obviously important and urgent to make a detailed investigation of the performance of such future detectors. In this paper we focus on how far we can probe the cosmic supernova rate by SRN observations at Gd-SK and at the hypothetical Gd-loaded Hyper-Kamiokande (Gd-HK) detector or Gd-loaded Underground Nucleon Decay and Neutrino

Observatory (Gd-UNO). Because the expected event rate of SRNs is about $1\text{--}2 \text{ yr}^{-1}$ in the detectable energy range (10–30 MeV) using a detector with the size of SK, it would be quite difficult to obtain the spectral information of SRNs, even if we observed for 5 years. On the other hand, with the currently proposed megaton-class detectors such as HK and UNO, we can expect to obtain a great deal of information about the SRN spectrum, which will be useful for inferring the SFR- z relation. Using the Monte Carlo (MC) method, we simulate an expected SRN signal at these future detectors, and then we analyze these hypothetical data with a few free parameters and discuss implications from future SRN observations.

This paper is organized as follows. In § 2 we give the formulation for calculating the SRN flux and discuss several models that are adopted in our calculations, and in § 3 we show the results of our calculation with some reference models. In § 4 the MC simulation of the expected signal at the future Gd-loaded detectors, which is generated from the reference models, is presented, and then we analyze these hypothetical data using several free parameters concerning the cosmic SFR. Finally, we discuss other possibilities in § 5.

2. FORMULATION AND MODELS

2.1. Formulation

The present number density of SRN ($\bar{\nu}_e$), whose energy is in the interval $E_\nu \sim E_\nu + dE_\nu$, emitted in the redshift interval $z \sim z + dz$, is given by

$$\begin{aligned} dn_\nu(E_\nu) &= R_{\text{SN}}(z)(1+z)^3 \frac{dt}{dz} dz \frac{dN_\nu(E'_\nu)}{dE'_\nu} dE'_\nu (1+z)^{-3} \\ &= R_{\text{SN}}(z) \frac{dt}{dz} dz \frac{dN_\nu(E'_\nu)}{dE'_\nu} (1+z) dE_\nu, \end{aligned} \quad (1)$$

where $E'_\nu = (1+z)E_\nu$ is the energy of neutrinos at redshift z , which is now observed as E_ν ; $R_{\text{SN}}(z)$ represents the supernova rate per comoving volume at z , and hence the factor $(1+z)^3$ should be multiplied to obtain the rate per physical volume at that time; dN_ν/dE_ν is the number spectrum of neutrinos emitted by one supernova explosion; and the factor $(1+z)^{-3}$ comes from the expansion of the universe. The Friedmann equation gives the relation between t and z as

$$\frac{dz}{dt} = -H_0(1+z) \sqrt{(1+\Omega_m z)(1+z)^2 - \Omega_\Lambda(2z+z^2)}, \quad (2)$$

and we adopt the standard Λ CDM cosmology ($\Omega_m = 0.3, \Omega_\Lambda = 0.7$, and $H_0 = 70 h_{70} \text{ km s}^{-1} \text{ Mpc}^{-1}$).¹ We now obtain the differential number flux of SRNs, dF_ν/dE_ν , using the relation $dF_\nu/dE_\nu = c dn_\nu/dE_\nu$:

$$\begin{aligned} \frac{dF_\nu}{dE_\nu} &= \frac{c}{H_0} \int_0^{z_{\text{max}}} R_{\text{SN}}(z) \frac{dN_\nu(E'_\nu)}{dE'_\nu} \\ &\quad \times \frac{dz}{\sqrt{(1+\Omega_m z)(1+z)^2 - \Omega_\Lambda(2z+z^2)}}, \end{aligned} \quad (3)$$

where we assume that gravitational collapses began at the redshift $z_{\text{max}} = 5$.

2.2. Model for Cosmic Star Formation Rate

¹ Although we use the specific cosmological model here, the SRN flux itself is completely independent of such cosmological parameters, as long as we use observationally inferred SFR models (see their cancellation between eqs. [3] and [4]), as already discussed in Ando et al. (2003).

As our reference model for the SFR, we adopt a model that is based on recent progressive results of rest-frame UV, NIR H α , and FIR/submillimeter observations; a simple functional form for the SFR per unit comoving volume is given as (Porciani & Madau 2001)

$$\psi_*(z) = 0.32 h_{70} \frac{\exp(3.4z)}{\exp(3.8z) + 45} M_\odot \text{ yr}^{-1} \text{ Mpc}^{-3} \times \frac{\sqrt{(1 + \Omega_m z)(1 + z)^2 - \Omega_\Lambda (2z + z^2)}}{(1 + z)^{3/2}}. \quad (4)$$

Figure 1 shows the SFR $\psi_*(z)$ with the various data points from rest-frame UV (Lilly et al. 1996; Madau et al. 1996; Steidel et al. 1999), H α line (Gallego et al. 1995; Gronwall 1998; Tresse & Maddox 1998), and FIR/submillimeter (Flores et al. 1999; Hughes et al. 1998) observations; these data points are not corrected for dust extinction. In the local

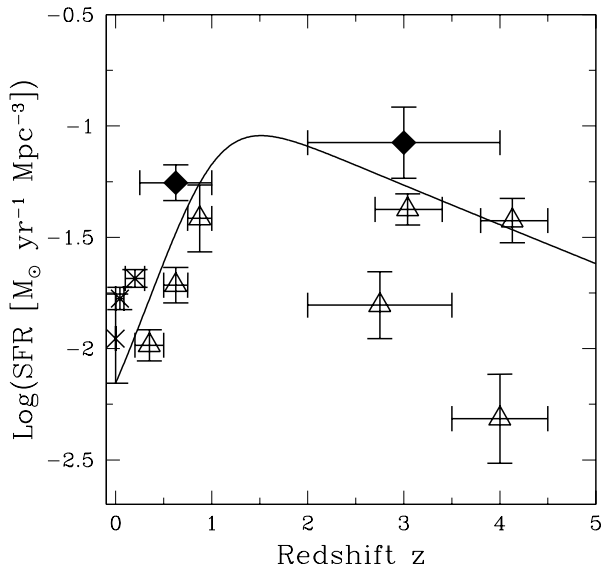


FIG. 1.— Cosmic star formation rate as a function of redshift. Data points are given by rest-frame UV (*open triangles*; Lilly et al. 1996; Madau et al. 1996; Steidel et al. 1999), NIR H α (*crosses*; Gallego et al. 1995; Gronwall 1998; Tresse & Maddox 1998), and FIR/submm (*filled diamonds*; Flores et al. 1999; Hughes et al. 1998) observations. The solid curve represents our reference model given by eq. (4). The standard Λ CDM cosmology is adopted ($\Omega_m = 0.3$, $\Omega_\Lambda = 0.7$, $H_0 = 70 \text{ km s}^{-1} \text{ Mpc}^{-1}$)

universe, all studies show that the comoving SFR monotonically increases with z out to a redshift of at least 1. Our reference model (eq. [4]) is consistent with mildly dust-corrected UV data at low redshift; on the other hand, it may underestimate the results of the other wave band observations. In our previous paper (Ando et al. 2003), we investigated the dependence on the several adopted SFR models, which were only different at high-redshift regions ($z \gtrsim 1.5$); our reference model (4) was referred to as the “SF1” model there. We showed that the SRN flux at $E_\nu > 10 \text{ MeV}$ is highly insensitive to the difference among the SFR models (owing to the energy redshift, as discussed in § 3.1), and therefore we do not repeat such discussions in the present paper.

We obtain the supernova rate ($R_{\text{SN}}(z)$) from the SFR by assuming the Salpeter IMF ($\phi(m) \propto m^{-2.35}$) with a lower cutoff

around $0.5 M_\odot$, and that all stars with $M > 8 M_\odot$ explode as core-collapse supernovae, i.e.,

$$R_{\text{SN}}(z) = \frac{\int_{8 M_\odot}^{125 M_\odot} dm \phi(m)}{\int_0^{125 M_\odot} dm m \phi(m)} \psi_*(z) = 0.0122 M_\odot^{-1} \psi_*(z). \quad (5)$$

The resulting local supernova rate agrees within errors with the observed value of $R_{\text{SN}}(0) = (1.2 \pm 0.4) \times 10^{-4} h_{70}^3 \text{ yr}^{-1} \text{ Mpc}^{-3}$ (e.g., Madau, della Valle, & Panagia 1998a and references therein). In fact, the totally time-integrated neutrino spectrum from massive stars ($\gtrsim 30 M_\odot$) could be very different from the models that we use (and give in the next subsection), possibly because of, e.g., black hole formation. However, the conversion factor appearing in equation (5) is highly insensitive to the upper limit of the integral in the numerator; for instance, if we change the upper limit in the numerator to $25 M_\odot$, the factor becomes $0.010 M_\odot^{-1}$, which is only slightly different from the value in equation (5).

2.3. Neutrino Spectrum from Supernova Explosions

For the neutrino spectrum from each supernova, we adopt three reference models by different groups, i.e., simulations by the Lawrence Livermore (LL) group (Totani et al. 1998) and Thompson, Burrows, & Pinto (2003, hereafter TBP), and the MC study of spectral formation by Keil, Raffelt, & Janka (2003, hereafter KRJ). In this field, however, the most serious problem is that the recent sophisticated hydrodynamic simulations have not obtained the supernova explosion itself; the shock wave cannot penetrate the entire core. Therefore, many points still remain controversial, e.g., the average energy ratio among neutrinos of different flavors, or how the gravitational binding energy is distributed to each flavor. All these problems are quite serious for our estimation, since the binding energy released as $\bar{\nu}_e$ changes the normalization of the SRN flux, and the average energy affects the SRN spectral shape. Thus, we believe that these three models from different groups will be complementary.

The numerical simulation by the LL group (Totani et al. 1998) is considered to be the most appropriate for our estimation, because it is the only model that succeeded in obtaining a robust explosion and in calculating the neutrino spectrum during the entire burst ($\sim 15 \text{ s}$). According to their calculation, the average energy difference between $\bar{\nu}_e$ and ν_x , where ν_x represent the nonelectron-flavor neutrinos and antineutrinos, was rather large and the complete equipartition of the binding energy was realized $L_{\nu_e} = L_{\bar{\nu}_e} = L_{\nu_x}$, where L_{ν_α} represents the released gravitational energy as α -flavor neutrinos. The neutrino spectrum obtained by their simulation is well fitted by a simple formula, which was originally given by KRJ as

$$\frac{dN_\nu}{dE_\nu} = \frac{(1 + \beta_\nu)^{1 + \beta_\nu} L_\nu}{\Gamma(1 + \beta_\nu) \bar{E}_\nu^2} \left(\frac{E_\nu}{\bar{E}_\nu} \right)^{\beta_\nu} e^{-(1 + \beta_\nu) E_\nu / \bar{E}_\nu}, \quad (6)$$

where \bar{E}_ν is the average energy; the values of the fitting parameters for the $\bar{\nu}_e$ and ν_x spectrum are summarized in Table 1.

Although the LL group succeeded in obtaining a robust explosion, their result has recently been criticized because it lacked many relevant neutrino processes that are now recognized as important. Thus, we adopt the recent result of another hydrodynamic simulation, the TBP one, which included all the relevant neutrino processes, such as neutrino

TABLE 1. FITTING PARAMETERS FOR SUPERNOVA NEUTRINO SPECTRUM

Model	Mass (M_{\odot})	$\bar{E}_{\bar{\nu}_e}$ (MeV)	\bar{E}_{ν_x} (MeV)	$\beta_{\bar{\nu}_e}$	β_{ν_x}	$L_{\bar{\nu}_e}$ (ergs)	L_{ν_x} (ergs)	Reference
LL	20	15.4	21.6	3.8	1.8	4.9×10^{52}	5.0×10^{52}	1
TBP	11	11.4	14.1	3.7	2.2	2
	15	11.4	14.1	3.7	2.2	2
	20	11.9	14.4	3.6	2.2	2
KRJ	...	15.4	15.7	4.2	2.5	3

REFERENCES. — (1) Totani et al. 1998; (2) Thompson et al. 2003; (3) Keil et al. 2003.

bremsstrahlung and neutrino-nucleon scattering with nucleon recoil. Their calculation obtained no explosion, and the neutrino spectrum ends at 0.25 s after core bounce. In the strict sense, we cannot use their result as our reference model because the fully time-integrated neutrino spectrum is definitely necessary in our estimate. However, we adopt their result in order to confirm the effects of recent sophisticated treatments of neutrino processes in the supernova core on the SRN spectrum. The TBP calculations include three progenitor mass models, i.e., 11, 15, and $20M_{\odot}$; all of these models are well fitted by equation (6), and the fitting parameters are summarized in Table 1. The average energy for both $\bar{\nu}_e$ and ν_x is much smaller than that by the LL calculation. Although we do not show this in Table 1, it was also found that at least for the early phase of the core-collapse, the complete equipartition of the gravitational binding energy for each flavor was not realized. However, it is quite unknown whether these trends hold during the entire burst. In this study, we adopt the average energy given in Table 1 as our reference model, while we assume perfect equipartition between flavors, i.e., $L_{\bar{\nu}_e} = L_{\nu_x} = 5.0 \times 10^{52}$ ergs.

In addition, we also use the model by KRJ. Their calculation did not couple with the hydrodynamics, but it focused on the spectral formation of neutrinos of each flavor using an MC simulation. Therefore, the static model was assumed as a background of neutrino radiation, and we use their ‘‘accretion phase model II,’’ in which the neutrino transfer was solved in the background of a 150 ms postbounce model by way of a general relativistic simulation. The fitting parameters for their MC simulation is also summarized in Table 1. Unlike the previous two calculations, their result clearly shows that the average energy of ν_x is very close to that of $\bar{\nu}_e$. It also indicates that the equipartition among each flavor was not realized, but rather $L_{\nu_e} \simeq L_{\bar{\nu}_e} \simeq 2L_{\nu_x}$. However also in this case, since the totally time-integrated neutrino flux is unknown from such temporary information, we assume perfect equipartition, $L_{\bar{\nu}_e} = L_{\nu_x} = 5.0 \times 10^{52}$ ergs, as well as that the average energies are the same as those in Table 1.

2.4. Neutrino Spectrum after Neutrino Oscillation

The original $\bar{\nu}_e$ spectrum is different from what we observe as $\bar{\nu}_e$ at Earth, owing to the effect of neutrino oscillation. Since the specific flavor neutrinos are not mass eigenstates, they mix with other flavor neutrinos during their propagation. The behavior of flavor conversion inside the supernova envelope is well understood, because the relevant mixing angles and mass square differences are fairly well determined by recent solar, atmospheric, and reactor neutrino experiments. The remaining ambiguities concerning the neutrino oscillation parameters are the value of θ_{13} , which is only weakly con-

strained ($\sin^2 \theta_{13} \lesssim 0.1$; Apollonio et al. 1999), and the type of mass hierarchy, i.e., normal ($m_1 \ll m_3$) or inverted ($m_1 \gg m_3$). We first discuss the case of normal mass hierarchy as our standard model; in this case, the value of θ_{13} is irrelevant. The case of inverted mass hierarchy is addressed in § 5.3. In addition, other exotic mechanisms, such as resonant spin-flavor conversion (see Ando & Sato 2003b and references therein) and neutrino decay (Ando 2003), which possibly change the SRN flux and spectrum, might work in reality. However, we do not consider such possibilities in this study.

The produced $\bar{\nu}_e$ at the supernova core are coincident with the lightest mass eigenstate $\bar{\nu}_1$ owing to the large matter potentials. Since this state $\bar{\nu}_1$ is the lightest also in vacuum, there are no resonance regions in which one mass eigenstate can change into another state, and therefore $\bar{\nu}_e$ at production arrives at the stellar surface as $\bar{\nu}_1$. Thus, the $\bar{\nu}_e$ spectrum observed by the distant detector is

$$\begin{aligned} \frac{dN_{\bar{\nu}_e}}{dE_{\bar{\nu}_e}} &= |U_{e1}|^2 \frac{dN_{\bar{\nu}_1}}{dE_{\bar{\nu}_1}} + |U_{e2}|^2 \frac{dN_{\bar{\nu}_2}}{dE_{\bar{\nu}_2}} + |U_{e3}|^2 \frac{dN_{\bar{\nu}_3}}{dE_{\bar{\nu}_3}} \\ &= |U_{e1}|^2 \frac{dN_{\bar{\nu}_e}^0}{dE_{\bar{\nu}_e}} + (1 - |U_{e1}|^2) \frac{dN_{\nu_x}^0}{dE_{\nu_x}}, \end{aligned} \quad (7)$$

where the quantities with superscript 0 represent those at production, $U_{\alpha i}$ is the mixing matrix element between the α -flavor state and i th mass eigenstate, and observationally $|U_{e1}|^2 = 0.7$. In other words, 70% of the original $\bar{\nu}_e$ survives; on the other hand, the remaining 30% comes from the other component ν_x . Therefore, both the original $\bar{\nu}_e$ and ν_x spectra are necessary for the estimation of the SRN flux and spectrum; since the original ν_x spectrum is generally harder than that of the original $\bar{\nu}_e$, as shown in Table 1, the flavor mixing is expected to harden the detected SRN spectrum.

3. FLUX AND EVENT RATE OF SUPERNOVA RELIC NEUTRINOS

3.1. Flux of Supernova Relic Neutrinos

The SRN flux can be calculated by equation (3) with our reference models given in § 2. Figure 2 shows the SRN flux as a function of neutrino energy for the three supernova models, LL, TBP, and KRJ. The flux of atmospheric $\bar{\nu}_e$, which becomes background events for SRN detection, is shown in the same figure (Gaisser, Stanev, & Barr 1988; Barr, Gaisser, & Stanev 1989). The SRN flux peaks at $\lesssim 5$ MeV, and around this peak, the TBP model gives the largest SRN flux because the average energy of the original $\bar{\nu}_e$ is considerably smaller than in the other two models but the total luminosity is assumed to be the same. On the other hand, the model gives a smaller contribution at high-energy regions, $E_{\nu} > 10$ MeV. In contrast, the high-energy tail of the SRN flux with the LL model extends farther than with the other models,

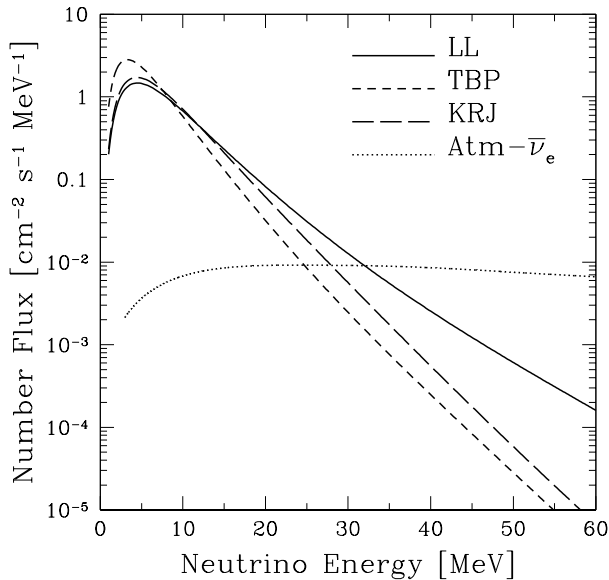


FIG. 2.— SRN flux calculated with three reference models of original neutrino spectrum: LL (Totani et al. 1998), TBP, and KRJ. The flux of atmospheric neutrinos (Gaisser et al. 1988; Barr et al. 1989) is also shown for comparison.

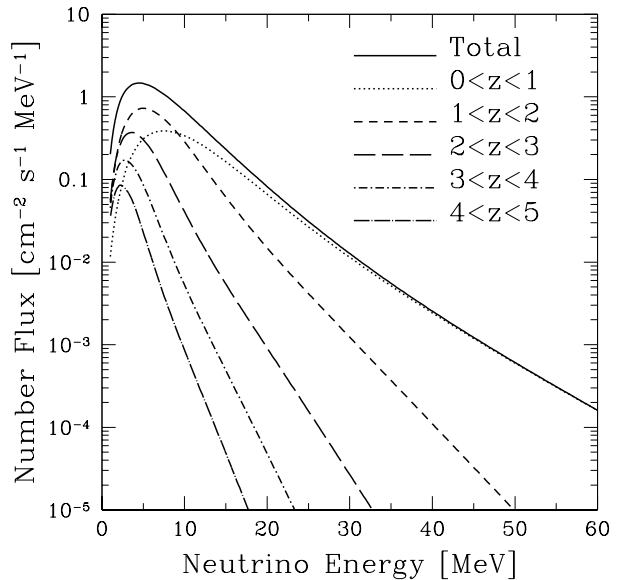


FIG. 3.— SRN flux from various redshift ranges. LL is adopted as the supernova model.

and it gives flux more than 1 mag larger at $E_\nu = 60$ MeV. This is because the high-energy tail was mainly contributed by the harder component of the original neutrino spectrum; in the case of the LL calculation, the average energy of the harder component ν_x is significantly larger than that of the other two calculations, as shown in Table 1. We show the values of the SRN flux integrated over the various energy ranges in Table 2.

(In the following, we refer only to the upper part of Table 2; the values in the lower part are discussed in § 5.3.) The total flux is expected to be $11\text{--}16\text{ cm}^{-2}\text{ s}^{-1}$ for our reference models, although this value is quite sensitive to the shape of the assumed SFR, especially at high- z . The energy range in which we are more interested is high-energy regions such as $E_\nu > 19.3$ MeV and $E_\nu > 11.3$ MeV, because as discussed below, the background events are less critical and the reaction cross section increases as $\propto E_\nu^2$. In such a range, the SRN flux is found to be $1.3\text{--}2.3\text{ cm}^{-2}\text{ s}^{-1}$ ($E_\nu > 11.3$ MeV) and $0.14\text{--}0.46\text{ cm}^{-2}\text{ s}^{-1}$ ($E_\nu > 19.3$ MeV). Thus, the uncertainty about the supernova neutrino spectrum and its luminosity gives at least a factor 2–4 ambiguity to the expected SRN flux in the energy region of our interest.

Figure 3 shows the contribution by supernova neutrinos emitted from various redshift ranges. At high-energy region $E_\nu > 10$ MeV, the dominant flux comes from the local supernovae ($0 < z < 1$), while the low-energy side is mainly contributed by the high-redshift events ($z > 1$). This is because the energy of neutrinos that were emitted from a supernova at redshift z is reduced by a factor of $(1+z)^{-1}$ reflecting the expansion of the universe, and therefore high-redshift supernovae only contribute to low-energy flux. We also show the energy-integrated flux from each redshift range in Table 2 in the case of the LL supernova model. From the table, it is found that in the energy range of our interest, more than 70% of the flux comes from local supernova explosions at $z < 1$,

while the high-redshift ($z > 2$) supernova contribution is very small.

3.2. Event Rate at Water Cerenkov Detectors

The water Cerenkov neutrino detectors have greatly succeeded in probing the properties of neutrinos as elementary particles, such as neutrino oscillation. The SK detector is one of these detectors, and its large fiducial volume (22.5 kton) might enable us to detect the diffuse background of SRNs. Furthermore, much larger water Cerenkov detectors such as HK and UNO are being planned. SRN detection is most likely with the inverse β -decay reaction with protons in water, $\bar{\nu}_e p \rightarrow e^+ n$, and its cross section is precisely understood (Vogel & Beacom 1999; Strumia & Vissani 2003). In our calculation, we use the trigger threshold of SK-I (before the accident).

The expected event rates at such detectors are shown in Figures 4 and 5 in units of $(22.5\text{ kton yr})^{-1}\text{ MeV}^{-1}$; with SK, it takes a year to obtain the shown SRN spectrum, while with HK and UNO, much less time [$1\text{ yr} \times (22.5\text{ kton}/V_{\text{fid}})$, where V_{fid} is the fiducial volume of HK or UNO] is necessary because of their larger fiducial volume. Figure 4 compares the three models of the original supernova neutrino spectrum, and Figure 5 shows the contribution to the total event rate from each redshift range. In Table 2 we summarize the event rate integrated over various energy ranges for three supernova models. The expected event rate is $0.97\text{--}2.3\text{ (22.5 kton yr)}^{-1}$ for $E_e > 10$ MeV and $0.25\text{--}1.0\text{ (22.5 kton yr)}^{-1}$ for $E_e > 18$ MeV. This clearly indicates that if the background events that hinder the detection are negligible, the SK has already reached the required sensitivity for detecting SRNs; with the future HK and UNO, a statistically significant discussion would be possible. This also shows that the current shortage of our knowledge concerning the original supernova neutrino spectrum and luminosity gives at least a factor of 2 ($E_\nu > 10$ MeV) to 4 ($E_\nu > 18$ MeV) uncertainty to the event rate at the high-

TABLE 2. FLUX AND EVENT RATE OF SUPERNOVA RELIC NEUTRINOS

Model	Redshift Range	Flux [$\text{cm}^{-2} \text{s}^{-1}$]			Event Rate [(22.5 kton yr) $^{-1}$]	
		Total	$E_\nu > 11.3 \text{ MeV}$	$E_\nu > 19.3 \text{ MeV}$	$E_e > 10 \text{ MeV}$	$E_e > 18 \text{ MeV}$
LL	Total	11.7	2.3	0.46	2.3	1.0
	$0 < z < 1^a$	4.1 (35.3)	1.6 (70.9)	0.39 (85.2)	1.7 (77.5)	0.9 (87.5)
	$1 < z < 2^a$	4.9 (42.0)	0.6 (26.3)	0.06 (14.0)	0.5 (20.6)	0.1 (11.9)
	$2 < z < 3^a$	1.8 (15.1)	0.1 (2.5)	0.0 (0.7)	0.0 (1.7)	0.0 (0.5)
	$3 < z < 4^a$	0.6 (5.3)	0.0 (0.2)	0.0 (0.0)	0.0 (0.1)	0.0 (0.0)
	$4 < z < 5^a$	0.2 (2.1)	0.0 (0.0)	0.0 (0.0)	0.0 (0.0)	0.0 (0.0)
TBP	Total	16.1	1.3	0.14	0.97	0.25
KRJ	Total	12.7	2.0	0.28	1.7	0.53
Inverted Mass Hierarchy with Large θ_{13}						
LL	Total	9.4	3.1	0.94	3.8	2.3
TBP	Total	13.8	1.9	0.30	1.6	0.58
KRJ	Total	12.4	2.2	0.38	2.0	0.76

NOTE. — Values in the upper part are evaluated for the case of normal mass hierarchy (or inverted mass hierarchy with sufficiently small θ_{13} , i.e., $\sin^2 2\theta_{13} \lesssim 10^{-5}$), which we use as our standard model. On the other hand, values in the lower part are applicable only when the value of θ_{13} is large enough to induce completely adiabatic resonance, i.e., $\sin^2 2\theta_{13} \gtrsim 10^{-3}$, in the case of inverted mass hierarchy.

^aContributions from each redshift range to the total ($0 < z < 5$) value are shown in parentheses as percentages.

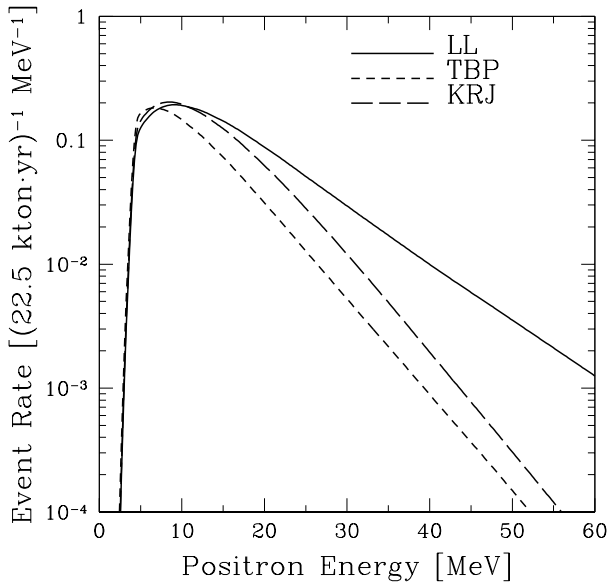


FIG. 4.—Event rate at water Cerenkov detectors in units of $(22.5 \text{ kton yr})^{-1} \text{ MeV}^{-1}$ for three supernova models.

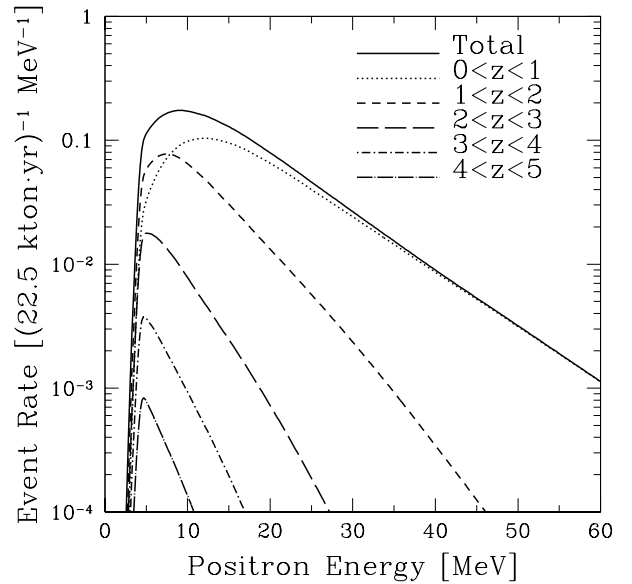


FIG. 5.—Event rate at water Cerenkov detectors in units of $(22.5 \text{ kton yr})^{-1} \text{ MeV}^{-1}$ from various redshift ranges. LL is adopted as the supernova model.

energy range (actual detection range). We also summarize the contribution from each redshift range in the same table, especially for the calculation with the LL model. The bulk of the detected events will come from the local universe ($z < 1$), but the considerable flux is potentially attributed to the range $1 < z < 2$.

3.3. Comparison with Other Studies and Current Observational Limits

There are many past theoretical researches concerning the SRN flux estimation based on a theoretically/observationally modeled cosmic SFR (Totani et al. 1996; Malaney 1997;

Hartmann & Woosley 1997; Ando et al. 2003). Here we briefly compare our results obtained in § 3.1 and § 3.2 with these past analyses. Our basic approach in the present paper is the same as that in Ando et al. (2003), in which the LL supernova model was adopted. Thus the values for the LL model given in Table 2 are almost the same as those in Ando et al. (2003). Two other studies (Totani et al. 1996; Hartmann & Woosley 1997) also used a similar SFR- z relation at low-redshift, and therefore their results are very consistent with the present one (the LL model) at high-energy region $E_\nu > 10 \text{ MeV}$. Since the SFR model adopted by Malaney (1997) gave a rather lower value at low-redshift, the result-

ing SRN flux at high-energy regions was about a factor 2 smaller than our LL model or the other ones (Totani et al. 1996; Hartmann & Woosley 1997; Ando et al. 2003). Thus, our calculation with the LL supernova model gives values quite consistent with past studies within a factor of 2, but all of those studies used the supernova model that is very similar to the LL model. In fact, the present study is the first one to investigate the dependence on the adopted supernova models, by using the various original spectra of the different groups (LL, TBP, and KRJ). As already mentioned in § 3.1, it was found that the ambiguity concerning the original neutrino spectrum varies the resulting value of the flux by at least a factor of 2.

In addition, there are several other studies on the SRN flux (Totani & Sato 1995; Kaplinghat et al. 2000; Fukugita & Kawasaki 2003). As for Totani & Sato (1995), the authors used a constant supernova rate model in order to investigate the dependence on cosmological parameters; they gave a very large value ($\sim 3 \text{ cm}^{-2} \text{ s}^{-1}$ at $E_\nu > 19.3 \text{ MeV}$), which is already excluded observationally, because they adopted a rather large supernova rate. Concerning the other two studies, since neither of them gives a specific value for the SRN flux, we cannot compare ours with theirs; they focused on giving theoretical upper limit (Kaplinghat et al. 2000) or probing the cosmic SFR with the current observational upper limit by SK (Fukugita & Kawasaki 2003).

Observationally, the SK collaboration gave a very stringent upper limit to the SRN flux at $E_\nu > 19.3 \text{ MeV}$, i.e., $1.2 \text{ cm}^{-2} \text{ s}^{-1}$ (90% CL; Malek et al. 2003). This number can be directly compared with our predictions summarized in Table 2. Our predicted values are 0.46, 0.14, and $0.28 \text{ cm}^{-2} \text{ s}^{-1}$ for the LL, TBP, and KRJ models, respectively. Thus, the current SK upper limit is about a factor 2.5–8.5 larger than our predictions with the reference model for the cosmic SFR, depending on the adopted original neutrino spectrum.

3.4. Background Events against Detection

In § 3.2 we calculated the expected SRN spectrum at the water Cerenkov detectors on Earth, but the actual detection is quite restricted because of the presence of other background events. There are atmospheric and solar neutrinos, antineutrinos from nuclear reactors, spallation products induced by cosmic-ray muons, and decay products of invisible muons (for a detailed discussion of these backgrounds, see Ando et al. 2003). For the pure-water Cerenkov detectors, there is no energy window in which the flux of any backgrounds is much smaller than the SRN flux.

However, as proposed by Beacom & Vagins (2003), if we use Gd-loaded detectors, the range 10–30 MeV would be an energy window because we can positively distinguish the $\bar{\nu}_e$ signal from other backgrounds such as solar neutrinos (ν_e), invisible muon events, and spallation products; this is realized by capturing neutrons that are produced by the $\bar{\nu}_e p$ interactions. Above 30 MeV, the SRN flux becomes smaller than the flux of atmospheric $\bar{\nu}_e$, as shown in Figure 2; because they are of the same flavor, it is in principle impossible to distinguish them from the SRN $\bar{\nu}_e$. On the other hand, below 10 MeV the reactor neutrinos ($\bar{\nu}_e$) are the dominant background in the case of SK or HK; because the flux of reactor neutrinos strongly depends on the detector site, it may be possible to further reduce this lower energy cutoff (10 MeV) in the case of UNO.

The neutron capture efficiency by Gd is estimated to be 90% with the proposed 0.2% mixture by mass of GdCl_3 in

water (Beacom & Vagins 2003), and subsequently 8 MeV gamma cascade occurs from the excited Gd. The single-electron energy equivalent to this cascade was found to be 3–8 MeV by careful simulation (Hargrove et al. 1995), and with the trigger threshold adopted in SK-I, only about 50% of such cascades can be detected actually. However, it is expected that SK-III, which will begin operation in mid-2006, will trigger at 100% efficiency above 3 MeV, with good trigger efficiency down to 2.5 MeV (Beacom & Vagins 2003). In that case most of the gamma cascades from Gd will be detected with their preceding signal of positrons. From this point on, we assume 100% efficiency; even if we abandon this assumption, it does not affect our physical conclusion, since the relevant quantity representing the detector performance is (fiducial volume) \times (time) \times (efficiency), which we call effective volume.

4. MONTE CARLO SIMULATION FOR FUTURE DETECTOR PERFORMANCE

In this section we predict the expected signal at future detectors, such as Gd-SK, Gd-HK, and Gd-UNO, using the MC method with our reference models. These pseudodata are then analyzed using several free parameters concerning the SFR. Although we focus on how far the SFR can be probed by SRN observation, the uncertainty from the supernova neutrino spectrum would give a fair amount of error. However, this problem can be solved if a supernova explosion occurs in our Galaxy; the expected event number is about 5000–10,000 at SK, when supernova neutrino burst occurs at 10 kpc, and it will enable a statistically significant discussion concerning the neutrino spectrum from supernova explosions. Even if there are no Galactic supernovae in the near future, remarkable development of the supernova simulation can be expected with the growth of computational resources and numerical technique. With such developments, the supernova neutrino spectrum and luminosity may be uncovered, and the ambiguity is expected to be reduced significantly. Thus, in this paper we assume that the supernova neutrino spectrum is well understood and that our reference models are fairly good representatives of nature; we analyze the SFR alone with several free parameters.

The basic procedure of our method is as follows. (1) We simulate the expected signal (spectrum) at a Gd-loaded detector in the range 10–30 MeV, assuming that there are no background events. In that process, we use our reference models for the generation of the SRN signal (eq. [4] for the SFR and the LL model as neutrino spectrum). (2) Then we analyze the SRN spectrum using the maximum likelihood method with two free parameters of the SFR and obtain a set of the best-fit values for those parameters; they are concerned with the supernova rate as

$$R_{\text{SN}}(z) = \begin{cases} R_{\text{SN}}^0(1+z)^\alpha & \text{for } z < 1, \\ 2^\alpha R_{\text{SN}}^0 & \text{for } z > 1, \end{cases} \quad (8)$$

where R_{SN}^0 represents the local supernova rate and α determines the slope of supernova rate evolution. Although it is recognized that the SFR- z relation increases from $z=0$ to $z=1$ from various observations using light, the actual numbers for the absolute value and the slope of the SFR- z relation are still a matter of controversy and independent confirmation, such as ours, is needed. We assume that the comoving SFR is constant at $z > 1$; even if we changed this assumption, the result would be the same because the bulk of the detected event comes from local supernovae. (3) We perform 10^3 such MC

simulations and obtain 10^3 independent sets of best-fit parameters. Then we discuss the standard deviation of the distributions of such best-fit parameter sets and the implications for the cosmic SFR.

4.1. Performance of the Gd-loaded Super-Kamiokande Detector

In this subsection we discuss the performance of Gd-SK for 5 years, or an effective volume of $22.5 \text{ kton} \times 5 \text{ yr}$. Because the expected event number is only ~ 10 , the parameters R_{SN}^0 and α cannot both be well determined at once. Therefore, we fix one of those parameters with some value inferred from other observations. First, the value of R_{SN}^0 was fixed to be $1.2 \times 10^{-4} \text{ yr}^{-1} \text{ Mpc}^{-3}$, which was inferred from the local supernova survey (Madau et al. 1998a), and we obtained the distribution of the best-fit values of parameter α . Figure 6 shows the expected SRN spectrum; points with error bars represent the result of one MC simulation, and the dashed histogram is the spectrum with the best-fit parameter ($\alpha = 2.97$). Thus, from one realization of the MC simulation, we obtain

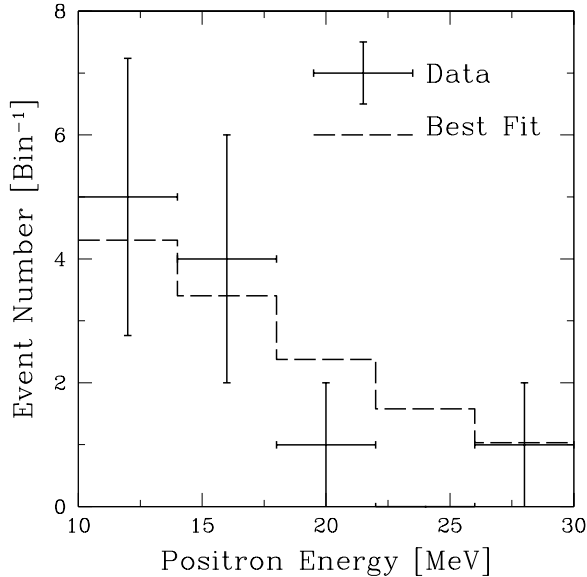


FIG. 6.— Expected SRN spectrum at a detector of effective volume $22.5 \text{ kton} \times 5 \text{ yr}$. The data points represent the result of MC simulation, and the error bars include statistical errors alone. These data generated by MC simulation were analyzed assuming $R_{\text{SN}}^0 = 1.2 \times 10^{-4} \text{ yr}^{-1} \text{ Mpc}^{-3}$, and using α as a free parameter. The best-fit value for α is 2.97 and it resulted in dashed histogram in this figure.

one best-fit parameter. The result of 10^3 MC simulations are shown in Figure 7 as a histogram of the distribution of best-fit parameters α (*solid histogram*). The average value of these 10^3 values for α is found to be 2.67, and the standard deviation is 0.80, i.e., $\alpha = 2.67 \pm 0.80$. A no-evolution (constant supernova rate) model would be excluded at the 3.3σ level from the SRN observation alone with an effective volume of $22.5 \text{ kton} \times 5 \text{ yr}$.

Then in turn, we fixed the value of α to be 2.9 in order to obtain the distribution of best-fit values for the local supernova rate R_{SN}^0 from the SRN observation. The result of 10^3 MC generations and analyses in this case is shown in Figure 8. The average value for R_{SN}^0 is $1.2 \times 10^{-4} \text{ yr}^{-1} \text{ Mpc}^{-3}$,

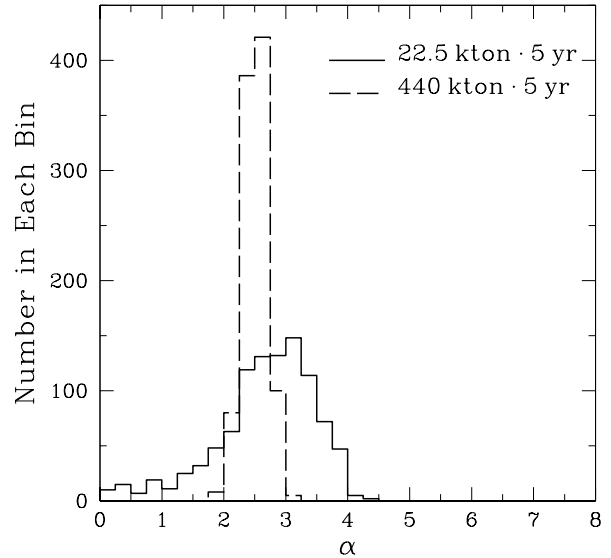


FIG. 7.— Distribution of 10^3 best-fit values for α , which are obtained from the analyses of each MC generation. The effective volume is $22.5 \text{ kton} \times 5 \text{ yr}$ for solid histogram, and $440 \text{ kton} \times 5 \text{ yr}$ for dashed histogram. The value of the local supernova rate is fixed to be $R_{\text{SN}}^0 = 1.2 \times 10^{-4} \text{ yr}^{-1} \text{ Mpc}^{-3}$.

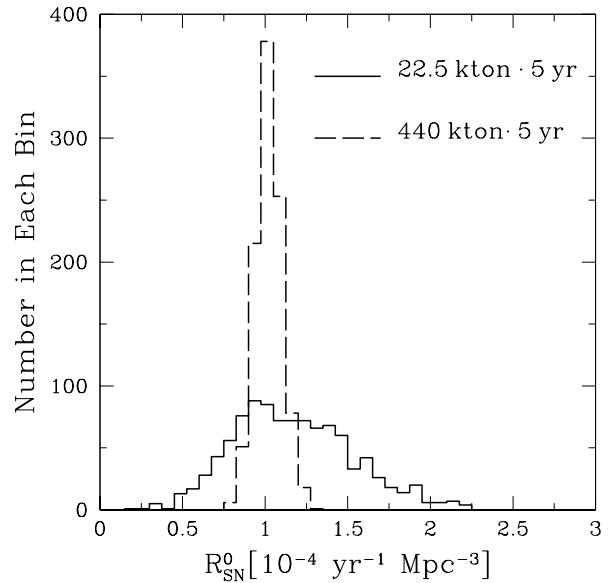


FIG. 8.— Distribution of 10^3 best-fit values for local supernova rate R_{SN}^0 , which are obtained from the analyses of each MC generation. The effective volume is $22.5 \text{ kton} \times 5 \text{ yr}$ for solid histogram, and $440 \text{ kton} \times 5 \text{ yr}$ for dashed histogram. The value of α is fixed to be 2.9.

and the standard deviation is $0.4 \times 10^{-4} \text{ yr}^{-1} \text{ Mpc}^{-3}$, i.e., $R_{\text{SN}}^0 = (1.2 \pm 0.4) \times 10^{-4} \text{ yr}^{-1} \text{ Mpc}^{-3}$.

The results obtained with the above calculations are summarized in Table 3. In Figure 9 we compare the supernova rate model in which the parameter is inferred from the MC simulations with the “true” reference model; the cases of

TABLE 3. EXPECTED SENSITIVITY OF FUTURE DETECTORS TO SUPERNOVA RATE MODEL

Detector	Effective Volume (22.5 kton yr)	Fixed Parameter	α	$\delta\alpha/(\alpha)$ (%)	R_{SN}^0 ($10^{-4} \text{ yr}^{-1} \text{ Mpc}^{-3}$)	$\delta R_{\text{SN}}^0 / \langle R_{\text{SN}}^0 \rangle$ (%)
SK	5	R_{SN}^0	2.7 ± 0.8	30.0	1.2 (fixed)	...
	5	α	2.9 (fixed)	...	1.2 ± 0.4	28.3
HK or UNO	97.8	R_{SN}^0	2.5 ± 0.2	7.8	1.2 (fixed)	...
	97.8	α	2.9 (fixed)	...	1.0 ± 0.1	7.7
	97.8	...	3.5 ± 1.3	36.7	0.88 ± 0.48	54.8

fixed R_{SN}^0 and α are shown in Figures 9a and 9b, respectively. The allowed region at the 1σ level is located between the two

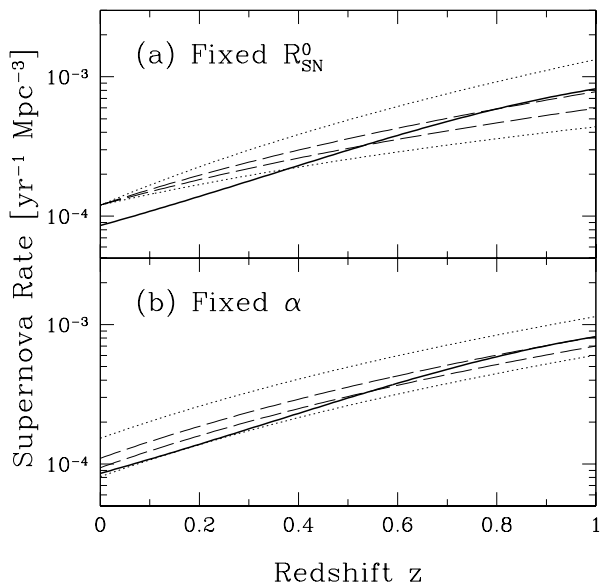


FIG. 9.— Supernova rate as a function of redshift. In both panels, solid curves represent our reference model. (a) The allowed region at the 1σ level, concerning the fitting parameter α with fixed R_{SN}^0 , is shown as the area between the two dotted curves for an effective volume of $22.5 \text{ kton} \times 5 \text{ yr}$ and as the area between the two dashed curves for an effective volume of $440 \text{ kton} \times 5 \text{ yr}$. (b) Same as (a) but for fitting parameter R_{SN}^0 with fixed α .

dotted curves, while the solid curve represents our reference model. Thus, with the Gd-SK detector we can roughly reproduce the supernova rate profile at $z < 1$ for 5 years operation, although it is still statistically insufficient.

4.2. Future Gd-loaded Megaton-Class Detectors

We consider future megaton-class detectors such as Gd-HK or Gd-UNO. With these detectors, the effective volume that we consider, $440 \text{ kton} \times 5 \text{ yr}$, is expected to be realized in several years from the start of their operation. First we did the same analysis adopted in the previous subsection, i.e., we fixed one of relevant parameters, α or R_{SN}^0 , and investigated the dependence on the remaining parameter. The values that we used for fixed parameters were the same as those given in the previous subsection. The result of these cases are also shown in Figures 7 and 8 as dashed histograms, which give $\alpha = 2.51 \pm 0.20$ and $R_{\text{SN}}^0 = (1.0 \pm 0.1) \times 10^{-4} \text{ yr}^{-1} \text{ Mpc}^{-3}$, respectively, and these values are also summarized in Table 3.

The statistical errors are considerably reduced compared with the case of $22.5 \text{ kton} \times 5 \text{ yr}$, because of the ~ 20 times larger effective volume. Thus, future magaton detectors will possibly pin down, within 10% statistical error, either the index of supernova rate evolution α or the local supernova rate R_{SN}^0 if the other is known in advance. The dashed curves in Figure 9 set the allowed region of the supernova rate at the 1σ level by the considered detectors, well reproducing the assumed model.

In principle, we can determine both parameters by SRN observation, because R_{SN}^0 is concerned with the absolute value of the flux alone but α is concerned with both the absolute value and the spectral shape; i.e., these two parameters are not degenerate with each other. Thus, we repeated the same procedure but without fixing the values of α or R_{SN}^0 . The distribution of 10^3 best-fit parameter sets of $(\alpha, R_{\text{SN}}^0)$ is shown in Figure 10 for a detector with an effective volume of $440 \text{ kton} \times 5 \text{ yr}$; the mean values and the standard deviations are $\alpha = 3.5 \pm 1.3$ and $R_{\text{SN}}^0 = (8.8 \pm 4.8) \times 10^{-5} \text{ yr}^{-1} \text{ Mpc}^{-3}$. Even

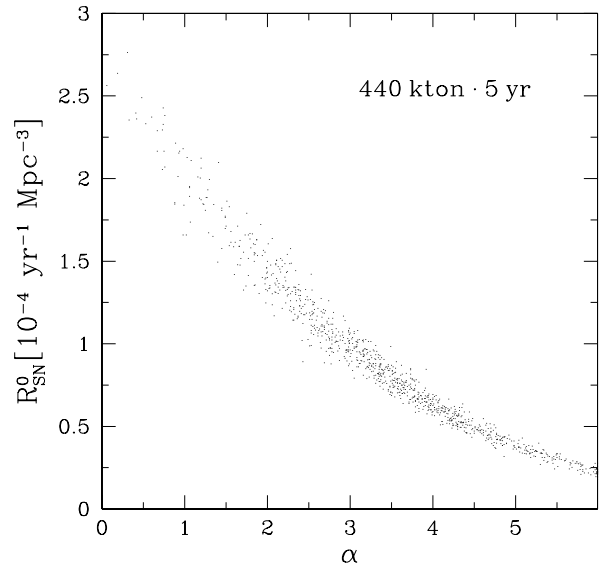


FIG. 10.— Distribution of 10^3 best-fit parameter sets $(\alpha, R_{\text{SN}}^0)$. Each dot represents the result of one MC generation and an accompanying analysis. The effective volume is $440 \text{ kton} \times 5 \text{ yr}$.

though the effective volume is as large as $440 \text{ kton} \times 5 \text{ yr}$, it is still insufficient for determining both parameters at once. For another trial, we also carried out the same MC simulations,

but using a hypothetical (and unrealistic) effective volume as large as $440 \text{ kton} \times 10^4 \text{ yr}$. In that case the free parameters are found to be quite well constrained at $\alpha = 3.68 \pm 0.03$ and $R_{\text{SN}}^0 = (7.11 \pm 0.09) \times 10^{-5} \text{ yr}^{-1} \text{ Mpc}^{-3}$.

5. DISCUSSION

5.1. Supernova Rate at High-Redshift Region

At the detection energy range 10–30 MeV that we have considered, the main contribution to the SRN event rate comes from low-redshift region $0 < z < 1$, as shown in Figure 5 and Table 2. However, if we can reduce the lower energy threshold E_{th} , we expect that the contribution of supernova neutrinos from high-redshift $z > 1$ becomes enhanced. The value of E_{th} is restricted to 10 MeV because at energy regions lower than this, there is a large background of reactor neutrinos; its removal is impossible with the current detection methods. Since the SK and HK detectors are and will be located at Kamioka in Japan, they are seriously affected by background neutrinos from many nuclear reactors. If some large-volume detectors were built at a location free from such background, the lower threshold energy could be reduced, enabling us to probe the high-redshift supernova rate. In this subsection, thus, we discuss the detector performance as a function of the value of E_{th} .

In Figure 11a we show three toy models of comoving density of supernova rate as a function of redshift. These models exactly coincide with each other at $z < 1$ (and also with the previous reference model represented by eq. [4]) but seriously differ at $z > 1$. We calculate the expected event number

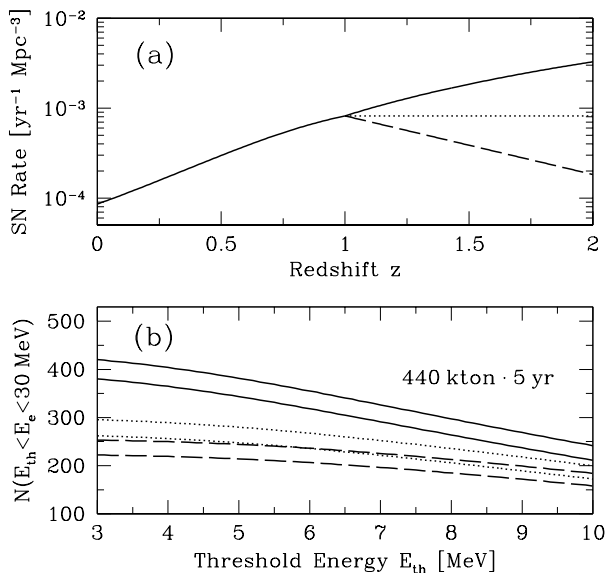


FIG. 11.— (a) Three toy models for comoving density of supernova rate as a function of redshift. (b) Expected event number N at $E_{\text{th}} < E_e < 30 \text{ MeV}$ as a function of E_{th} , for the fiducial volume of $440 \text{ kton} \times 5 \text{ yr}$. The line types correspond to those in (a). The upper and lower curves of each type represent $N + \sqrt{N}$ and $N - \sqrt{N}$, respectively; i.e., the area between the two curves is the allowed region at the 1σ level.

for $E_{\text{th}} < E_e < 30 \text{ MeV}$ at a detector with an effective volume of $440 \text{ kton} \times 5 \text{ yr}$, using these toy models, the LL spectrum, and trigger threshold expected at SK-III. The result is shown in Figure 11b. As expected, the discrepancy among the three

models becomes larger as we reduce the threshold energy. In particular, the model that produces larger numbers of supernovae at $z > 1$ (solid curve) is satisfactorily distinguishable in the case of sufficiently low E_{th} . This is because the larger supernova rate at high-redshift region $z > 1$ increases the fraction of its contribution to the SRN flux. On the other hand, the model with a lower supernova rate relatively increases the contribution from low-redshift region $z < 1$, and therefore the difference between constant (dotted curve) and decreasing model (dashed curve) is less prominent.

5.2. Probing Supernova Neutrino Properties

Until this point, we have assumed that the properties of supernova neutrinos, such as the average energy difference between flavors and luminosities of neutrinos of different flavors, will be quite well understood when future SRN detection comes within reach. However, this assumption itself is quite unclear because Galactic supernova explosions, which would give us rich information on the supernova neutrino spectrum and luminosity, may not occur by the time we are ready for the SRN detection. Furthermore, there is no assurance that the numerical experiments will succeed in obtaining the supernova explosion itself and predicting the supernova neutrino properties precisely by then. Thus, SRN observation might be the only probe of the supernova neutrino properties.

In this subsection, we discuss how far we can derive the supernova neutrino properties from SRN observation. We have already shown that even using data of $440 \text{ kton} \times 5 \text{ yr}$, at most only two free parameters can be satisfactorily constrained. Therefore, we now have to adopt another assumption such that the evolution of the supernova rate is quite well understood by future observations with the various planned satellites and telescopes. The procedure is basically the same as that of the previous section; i.e., we run 10^3 MC simulations and analyze these pseudodata to obtain the best-fit values for two free parameters, $\bar{E}_{\bar{\nu}_e}$ and $\bar{E}_{\nu_x}/\bar{E}_{\bar{\nu}_e}$. The values of β_{ν} and L_{ν} defined in equation (6) are assumed to be $\beta_{\bar{\nu}_e} = 4.0$, $\beta_{\nu_x} = 2.2$, and $L_{\bar{\nu}_e} = L_{\nu_x} = 5.0 \times 10^{52} \text{ ergs}$. As a result of such calculations, we obtain the distribution of the two parameters, which is characterized by $\bar{E}_{\bar{\nu}_e} = (15.9 \pm 1.3) \text{ MeV}$ and $\bar{E}_{\nu_x}/\bar{E}_{\bar{\nu}_e} = 1.5 \pm 0.4$; although this well reproduces the LL model, the errors are still very large. Considering that many uncertainties concerning the SFR estimate possibly remain even in future updated observations, the errors to these quantities would be much larger than the purely statistical ones given above.

5.3. Inverted Mass Hierarchy

Throughout the above discussion, we have assumed normal hierarchy of neutrino masses ($m_1 \ll m_3$). However, the case of inverted mass hierarchy has not been experimentally excluded yet, and we explore this possibility in this subsection. In this case, flavor conversions inside the supernova envelope change dramatically, compared with the normal mass hierarchy already discussed in § 2.4. Since $\bar{\nu}_3$ is the lightest, $\bar{\nu}_e$ are created as $\bar{\nu}_3$, owing to large matter potential. In that case, it is well known that at a so-called resonance point, there occurs a level crossing between $\bar{\nu}_1$ and $\bar{\nu}_3$ (for a more detailed discussion, see, e.g., Dighe & Smirnov 2000). At this resonance point, complete $\bar{\nu}_1 \leftrightarrow \bar{\nu}_3$ conversion occurs when the so-called adiabaticity parameter is sufficiently small compared to unity (it is said that resonance is “nonadiabatic”), while conversion never occurs when it is large (adiabatic resonance). The adiabaticity parameter γ is quite sensitive to the value of θ_{13} , i.e.,

$\gamma \propto \sin^2 2\theta_{13}$; when $\sin^2 2\theta_{13} \gtrsim 10^{-3}$ ($\sin^2 2\theta_{13} \lesssim 10^{-5}$), the resonance is known to be completely adiabatic (nonadiabatic) (Dighe & Smirnov 2000). When the resonance is completely nonadiabatic (because of small θ_{13}), the situation is the same as in the case of normal mass hierarchy already discussed in § 2.4 (because $\bar{\nu}_e$ at production become $\bar{\nu}_1$ at the stellar surface), and the $\bar{\nu}_e$ spectrum after oscillation is represented by equation (7). On the other hand, adiabatic resonance (due to large θ_{13}) forces $\bar{\nu}_e$ at production to become $\bar{\nu}_3$ when they escape from the stellar surface, and therefore the observed $\bar{\nu}_e$ spectrum is given by

$$\frac{dN_{\bar{\nu}_e}}{dE_{\bar{\nu}_e}} = |U_{e3}|^2 \frac{dN_{\bar{\nu}_e}^0}{dE_{\bar{\nu}_e}^0} + (1 - |U_{e3}|^2) \frac{dN_{\nu_x}^0}{dE_{\nu_x}^0} \simeq \frac{dN_{\nu_x}^0}{dE_{\nu_x}^0}. \quad (9)$$

The second equality follows from the fact that the value of $|U_{e3}|^2$ is constrained to be much smaller than unity from reactor experiments (Apollonio et al. 1999). Thus, equation (9) indicates that complete conversion takes place between $\bar{\nu}_e$ and ν_x . When the value of θ_{13} is large enough to induce adiabatic resonance ($\sin^2 2\theta_{13} \gtrsim 10^{-3}$), the obtained SRN flux and spectrum should be very different from ones obtained in §§ 3.1 and 3.2. The SRN flux and event rate in this case were calculated with equations (3) and (9), and the results are summarized in the lower part of Table 2. The values (with the LL model) shown in this table are consistent with the previous calculation by Ando & Sato (2003a), in which numerically calculated conversion probabilities were adopted with some specific oscillation parameter sets (which include a model with inverted mass hierarchy and $\sin^2 2\theta_{13} = 0.04$), as well as realistic stellar density profiles.

The total flux becomes $9.4\text{--}14 \text{ cm}^{-2} \text{ s}^{-1}$, somewhat smaller than the values given in the upper part of the same table, because the total flux is dominated by the low-energy region. The fluxes at $E_\nu > 19.3 \text{ MeV}$ are enhanced to be $0.30\text{--}0.94 \text{ cm}^{-2} \text{ s}^{-1}$, but this is still below the current 90% CL upper limit of $1.2 \text{ cm}^{-2} \text{ s}^{-1}$ obtained by the SK observation. The event rate at the future detectable energy range, $E_\nu > 10 \text{ MeV}$, is expected to become $1.6\text{--}3.8 \text{ yr}^{-1}$, which is considerably larger than the values in the case of normal mass hierarchy, $0.97\text{--}2.3 \text{ yr}^{-1}$. The increase (decrease) of the flux and event rate integrated over the high (total) energy region is due to the very high efficiency of the flavor conversion, $\nu_x \rightarrow \bar{\nu}_e$, inside the supernova envelope; because the original ν_x are expected to be produced with larger average energy as shown in Table 1, the efficient conversion makes the SRN spectrum harder, which enhances the flux and event rate at the high-energy region. Thus, if the inverted mass hierarchy, as well as the large value for θ_{13} , were realized in nature, SRN detection would be rather easier, compared with the other cases. Although we do not repeat the MC simulations that were introduced in § 4, the results can be easily inferred; the statistical errors in this case would be $\sim (3.8/2.3)^{1/2} = 1.3$ times smaller than the values given in Table 3, because they are inversely proportional to the square root of the event number.

6. CONCLUSIONS

In the present paper, we have investigated the flux and event rate of SRNs and discussed their implications for the cosmic SFR. Since SRNs are diffuse neutrino background emitted from past core-collapse supernova explosions, they contain fruitful information not only on the supernova neutrino spectrum itself but also on the supernova rate in the past and present universe, which is quite difficult to estimate because,

e.g., the problem of dust extinction is nontrivial. As reference models, we adopted the supernova rate model based on recent SFR observations (eq. [4]) and the supernova neutrino spectrum numerically calculated by three groups (LL, TBP, and KRJ). As a result of our calculations, the flux integrated over the entire energy region was found to be $12\text{--}16 \text{ cm}^{-2} \text{ s}^{-1}$, depending on the adopted supernova neutrino spectrum (Table 2). Although there is no energy window for the SRN detection at present owing to various background events, in the near future, it is expected that the energy region of $10\text{--}30 \text{ MeV}$ will be utilized for SRN detection. This is due to the technique of neutron capture by dissolved Gd. In the detection energy range $E_e > 10 \text{ MeV}$, the SRN event rate was found to be $0.97\text{--}2.3 \text{ yr}^{-1}$ at a detector with a fiducial volume of 22.5 kton (Table 2).

We also simulated the expected signal with one set of the reference models by using the Monte Carlo method and then analyzed these pseudodata with several free parameters, obtaining one set of best-fit values for them. MC simulations repeated 10^3 times gave 10^3 independent best-fit parameter sets, and we gave a statistical discussion using their distribution. First of all, we used parameterization such that $R_{\text{SN}}(z) = R_{\text{SN}}^0(1+z)^\alpha$, where R_{SN}^0 and α are free parameters, assuming that the supernova neutrino spectrum and luminosity are well understood by way of a future Galactic supernova neutrino burst or future development of the numerical supernova simulations. The obtained distribution for these two parameters was found to be represented by $\alpha = 2.7 \pm 0.8$, $\delta\alpha/\langle\alpha\rangle = 30\%$ and $R_{\text{SN}}^0 = (1.2 \pm 0.4) \times 10^{-4} \text{ yr}^{-1} \text{ Mpc}^{-3}$, $\delta R_{\text{SN}}^0/\langle R_{\text{SN}}^0\rangle = 28\%$ for a detector with an effective volume of $22.5 \text{ kton} \times 5 \text{ yr}$, and $\alpha = 2.5 \pm 0.2$, $\delta\alpha/\langle\alpha\rangle = 7.8\%$ and $R_{\text{SN}}^0 = (1.0 \pm 0.1) \times 10^{-4} \text{ yr}^{-1} \text{ Mpc}^{-3}$, $\delta R_{\text{SN}}^0/\langle R_{\text{SN}}^0\rangle = 7.7\%$ for a detector with an effective volume of $440 \text{ kton} \times 5 \text{ yr}$, where one of the parameters is fixed (Figs. 7 and 8; Table 3). The parameterized supernova rate models with the obtained parameter values are compared with the assumed reference model in Figure 9, and we found that the fitting model well reproduced the reference model. On the other hand, if we fix neither value for these two parameters, the expected errors become rather large at $\delta\alpha/\langle\alpha\rangle = 37\%$ and $\delta R_{\text{SN}}^0/\langle R_{\text{SN}}^0\rangle = 55\%$, even with an effective volume of $440 \text{ kton} \times 5 \text{ yr}$.

In addition, we explored several other possibilities in § 5. First, we discussed the dependence of the event number on the adopted lower cutoff energy. Although below 10 MeV there is a background of reactor neutrinos, their flux strongly depends on the detector sites, and the lower energy threshold E_{th} could possibly be reduced. We investigated the expected event number for $E_{\text{th}} < E_e < 30 \text{ MeV}$ as a function of E_{th} in Figure 11 for various toy models of supernova rate and found that the model that produces larger number of supernovae at $z > 1$ is satisfactorily distinguishable in the case of sufficiently small E_{th} . Second, the SRN spectrum as a potential probe of the supernova neutrino spectrum itself was investigated, because such an approach might be very important if there are no Galactic supernova explosions in the near future or no successful numerical supernova simulations. We discussed using the same MC procedure, but assuming that the supernova rate is quite well understood. Although the obtained distribution reproduces properties of the LL spectrum, the errors were still found to be large, and considering the uncertainties concerning the SFR, these errors are only lower limits; the actual errors would be much larger. Finally, the case of an inverted mass hierarchy was investigated. We showed that only

in the case in which $\sin^2 2\theta_{13} \gtrsim 10^{-5}$ the values of the SRN flux should be modified. The results in the case of completely adiabatic resonance, which is realized when $\sin^2 2\theta_{13} \gtrsim 10^{-3}$, are shown in the lower part of Table 2. In this case, it was found that the expected event rate would be enhanced to 1.6–3.8 yr^{-1} , although these values are still below the current up-

per bound; SRN detection would be more probable in this case.

This work was supported by a Grant-in-Aid for JSPS Fellows.

REFERENCES

- Ando, S. 2003, *Phys. Lett. B*, 570, 11
 Ando, S. & Sato, K. 2003a, *Phys. Lett. B*, 559, 113
 —. 2003b, *J. Cosmology Astropart. Phys.*, 10, 1
 Ando, S., Sato, K., & Totani, T. 2003, *Astropart. Phys.*, 18, 307
 Apollonio, M. et al. 1999, *Phys. Lett. B*, 466, 415
 Barr, G., Gaisser, T. K., & Stanev, T. 1989, *Phys. Rev. D*, 39, 3532
 Beacom, J. F. & Vagins, M. R. 2003, preprint (hep-ph/0309300)
 Bionta, R. M. et al. 1987, *Phys. Rev. Lett.*, 58, 1494
 Connolly, A., Szalay, A., Dickinson, M., Rao, M. S., & Brunner, R. 1997, *ApJ*, 486, L11
 Cowie, L., Songaila, A., Hu, E., & Cohen, J. 1996, *AJ*, 112, 839
 Dighe, A. S. & Smirnov, A. Yu. 2000, *Phys. Rev. D*, 62, 033007
 Flores, H. et al. 1999, *ApJ*, 517, 148
 Fukugita, M. & Kawasaki, M. 2003, *MNRAS*, 340, L7
 Gaisser, T. K., Stanev, T., & Barr, G. 1988, *Phys. Rev. D*, 38, 85
 Gallego, J., Zamorano, J., Aragón-Salamanca, A., & Rego, M. 1995, *ApJ*, 455, L1
 Glazebrook, K., Blake, C., Economou, F., Lilly, S., & Colless, M. 1999, *MNRAS*, 306, 843
 Gronwall, C. 1998, in *Proc. 33rd Rencontres de Moriond, Dwarf Galaxies and Cosmology*, ed. T. Thuan et al. (Gif-sur-Yvette: Editions Frontières), 41
 Hargrove, C. K., Blevins, I., Paterson, D., & Earle, E. D. 1995, *Nucl. Instrum. Methods A*, 357, 157
 Hartmann, D. H. & Woosley, S. E. 1997, *Astropart. Phys.*, 7, 137
 Hirata, K. et al. 1987, *Phys. Rev. Lett.*, 58, 1490
 Hughes, D. H. et al. 1998, *Nature*, 394, 241
 Kaplinghat, M., Steigman, G., & Walker, T. P. 2000, *Phys. Rev. D*, 62, 043001
 Keil, M. T., Raffelt, G. G., & Janka, H. T. 2003, *ApJ*, 590, 971 (KRJ)
 Lilly, S., Fèvre, O. L., Hammer, F., & Crampton, D. 1996, *ApJ*, 460, L1
 Madau, P., della Valle, M., & Panagia, N. 1998a, *MNRAS*, 297, 17
 Madau, P., Ferguson, H. C., Dickinson, M. E., Giavalisco, M., Steidel, C. C., & Fruchter, A. 1996, *MNRAS*, 283, 1388
 Madau, P., Pozzetti, L., & Dickinson, M. 1998b, *ApJ*, 498, 106
 Malaney, R. A. 1997, *Astropart. Phys.*, 7, 125
 Malek, M. et al. 2003, *Phys. Rev. Lett.*, 90, 061101
 Pascarelle, S. M., Lanzetta, K. M., & Fernandez-Soto, A. 1998, *ApJ*, 508, L1
 Porciani, C. & Madau, P. 2001, *ApJ*, 548, 522
 Sawicki, M. J., Lin, H., & Yee, H. K. C. 1997, *AJ*, 113, 1
 Somerville, R. S., Primack, J. R., & Faber, S. M. 2001, *MNRAS*, 320, 504
 Steidel, C. C., Adelberger, K. L., Giavalisco, M., Dickinson, M., & Pettini, M. 1999, *ApJ*, 519, 1
 Strigari, L. E., Kaplinghat, M., Steigman, G., & Walker, T. P. 2003, preprint (astro-ph/0312346)
 Strumia, A. & Vissani, F. 2003, *Phys. Lett. B*, 564, 42
 Thompson, T. A., Burrows, A., & Pinto, P. 2003, *ApJ*, 592, 434 (TBP)
 Totani, T. & Sato, K. 1995, *Astropart. Phys.*, 3, 367
 Totani, T., Sato, K., Dalhed, H. E., & Wilson, J. R. 1998, *ApJ*, 496, 216
 Totani, T., Sato, K., & Yoshii, Y. 1996, *ApJ*, 460, 303
 Tresse, L. & Maddox, S. 1998, *ApJ*, 495, 691
 Treyer, M., Ellis, R., Milliard, B., Donas, J., & Bridges, T. 1998, *MNRAS*, 300, 303
 Vogel, P. & Beacom, J. F. 1999, *Phys. Rev. D*, 60, 053003